Preparation and the physical properties of antiperovskite-type compounds $Cd_{1-x}In_xNNi_3$ $(0 \leq x \leq 0.2)$ and $Cd_{1-y}Cu_yNNi_3$ $(0 \leq y \leq 0.2)$*

He Bing(贺 兵)[a)b)†], Dong Cheng(董 成)[a)], Yang Li-Hong(杨立红)[a)], Ge Lin-Hui(葛林慧)[a)], Mu Li-Bin(慕利斌)[a)], Chen Xiao-Chao(陈晓超)[a)]

[a)] *National Laboratory for Superconductivity, Institute of Physics, Chinese Academy of Sciences, Beijing* 100190, *China*
[b)] *Luzhou Medical College, Luzhou* 646000, *China*

(Received 27 November 2011; revised manuscript received 6 January 2012)

Two series of $Cd_{1-x}In_xNNi_3$ $(0 \leq x \leq 0.2)$ and $Cd_{1-y}Cu_yNNi_3$ $(0 \leq y \leq 0.2)$ samples were prepared from CdO, In_2O_3, CuO, and nickel powders under NH_3 atmosphere at 773 K. The structural and physical properties were investigated by means of X-ray powder diffraction temperature-dependent resistivity and magnetic measurements. X-ray powder diffraction results showed that the $Cd_{1-x}In_xNNi_3$ and $Cd_{1-y}Cu_yNNi_3$ compounds have a typical antiperovskite structure, and the $CdNNi_3$, $Cd_{0.9}In_{0.1}NNi_3$, and $Cd_{0.9}Cu_{0.1}NNi_3$ compounds show metallic temperature-dependent resistivity and exhibit a Fermi liquid behavior at low temperature. In contrast to the paramagnetism previously reported, the $CdNNi_3$ sample exhibits very soft and weak ferromagnetism, and no superconductivity was found in the $Cd_{1-x}In_xNNi_3$ and $Cd_{1-y}Cu_yNNi_3$ samples down to 2 K. Each sample exhibited very soft and weak ferromagnetism, and the temperature dependence of the magnetization of the $Cd_{1-x}In_xNNi_3$ and $Cd_{1-y}Cu_yNNi_3$ samples can be well fitted to the combination of a Bloch term and a Curie–Weiss term.

Keywords: nitride, antiperovskite, weak ferromagnetism, Fermi liquid

PACS: 74.70.Dd, 75.50.Gg **DOI:** 10.1088/1674-1056/21/4/047401

1. Introduction

The discovery of superconductivity in $MgCNi_3$[1] has stimulated research on Ni-based antiperovskite compounds with a general formula $MXNi_3$, where M is a divalent or trivalent metal, and X is C or N. Many such carbides, i.e., $MCNi_3$ (M = Cd, Zn, Al, Ga, In, and so on)[2−6] have been studied. Among these materials, only the $CdCNi_3$ compounds demonstrate superconductivity with T_c = 3.4 K. $ZnCNi_3$ is a Pauli paramagnetic (PM) metal without onset of superconductivity down to 2 K. Both $AlCNi_3$ and $GaCNi_3$ take on strongly exchange-enhanced PM behaviors, while $In_{0.95}CNi_3$ behaves as a ferromagnetic (FM) metal below the Curie temperature (577 K).

In addition to carbides, many antiperovskite nitrides have been studied. Fe-based nitrides $MNFe_3$ (M = Fe, Mn, Au, Ag, Sn, Pd, Ni, Pt) exhibit interesting Invar-like behavior.[7−15] Mn–based nitrides $ANMn_3$ (A = Cu, Zn, Ga, Ge, etc) show large negative thermal expansion triggered by antiferromagnetic (AFM) or FM transitions.[16,17] Recently, several Ni-based antiperovskite nitrides, i.e., $ZnNNi_3$,[18] $InNNi_3$,[19] and $CdNNi_3$,[20] have been synthesized. $ZnNNi_3$ is the first nitrogen-containing superconducting material (T_c = 3 K) in the Ni-based perovskite series. $InNNi_3$ exhibits spin-glass-like behavior, whereas $CdNNi_3$ behaves as a PM metal.

Since Cd has the same valence state (+2) as Zn, $CdNNi_3$ and $ZnNNi_3$ should have similar electronic structures. Therefore, they are expected to show similar electrical and magnetic properties. However, the theoretical study has pointed out that the electron density of states (DOS) of $ZnNNi_3$ at the Fermi level (E_F) is higher than that of $CdNNi_3$.[21] In the framework of rigid band approximation, hole doping makes an enhancement in DOS at E_F, while electron doping depresses DOS at E_F. We conjectured that $CdNNi_3$ might become superconducting via suitable carrier doping. In this paper, we report the synthesis and physical properties of the $Cd_{1-x}In_xNNi_3$

*Project supported by the National Natural Science Foundation of China (Grant No. 20871119), the National Basic Research Program of China (973 Program) (Grant Nos. 2011CBA00112 and 2011CB808202), and the Natural Science Foundation of Luzhou Medical College.

†Corresponding author. E-mail: hebing@ssc.iphy.ac.cn

© 2012 Chinese Physical Society and IOP Publishing Ltd

($0 \leq x \leq 0.2$) and $Cd_{1-y}Cu_yNNi_3$ ($0 \leq y \leq 0.2$) compounds.

2. Experimental

CdO (>99%), In_2O_3 (>99%), CuO (>99%), and nickel powders (99.5%) were used as the starting materials. Two series of $Cd_{1-x}In_xNNi_3$ ($0 \leq x \leq 0.3$) and $Cd_{1-y}Cu_yNNi_3$ ($0 \leq y \leq 0.25$) samples were prepared by the solid–gas reactions of the starting materials with NH_3 (99.9% purity) at ambient pressure. An extra 20% CdO was added in order to compensate for evaporation during the reaction. The starting materials were thoroughly ground, and then put into alumina boats. The mixtures were heated in a tube furnace at 773 K for 10 h under static NH_3 atmosphere and subsequently furnace cooled to room temperature. During the heating process, fresh NH_3 gas was refilled six times to remove the H_2O vapor produced in the reaction. The obtained intermediate products are loose powders. To facilitate the resistivity and magnetic measurements, the intermediate products were reground thoroughly, pressed into pellets and sintered for another 10 h under the same reaction conditions.

The powder X-ray diffraction (PXRD) data of the samples were collected on a MXP18A-HF diffractometer with Cu Kα radiation at room temperature. The 2θ scan range was from 20° to 120° with a step size of 0.02° and a counting time of 2 s. Phase analyses of the samples were performed using a search–match operation on experimentally obtained peak files using the ICDD-PDF database and Jade 5.0 software. The lattice parameters of the samples were calculated using the least-square method with the help of the PowderX program.[22] The grain morphology and microstructure were obtained using a field emission scanning electron microscope (FE–SEM, FEI XL 30 S–FEG) and the chemical compositions of the samples were examined using an energy-dispersive X-ray spectroscopy (EDX) attachment. An Elementary Vario Micro Cube (Germany) elemental analyzer was employed to determine the nitrogen content.

The temperature dependence of electrical resistivity was measured using the four probe method in the temperature range 5 K–300 K. Magnetic measurements were performed employing a superconducting quantum interference device magnetometer (MPMS XL–7, Quantum Design) in the temperature range 2 K–300 K.

3. Results and discussion

PXRD patterns for the series of $Cd_{1-x}In_xNNi_3$ ($0 \leq x \leq 0.3$) samples are shown in Fig. 1. From Fig. 1, it can be seen that the samples with $x \leq 0.2$ are single phase, and all diffraction patterns can be well indexed to the antiperovskite-type structure with space group $Pm3m$. However, the diffraction peaks of the $Cd_{1-x}In_xNNi_3$ samples broadened abnormally when $x > 0.2$, indicating a possible phase separation. As shown in Fig. 1(b), the diffraction peaks shift towards lower angle regions as the indium content increases, suggesting that the effective radii of In are slightly larger than those of the Cd in the antiperovskites. The lattice parameter a of $Cd_{1-x}In_xNNi_3$ linearly increases from 3.8483 Å to 3.8511 Å (1 Å=0.1 nm) with increasing indium content (see Fig. 3).

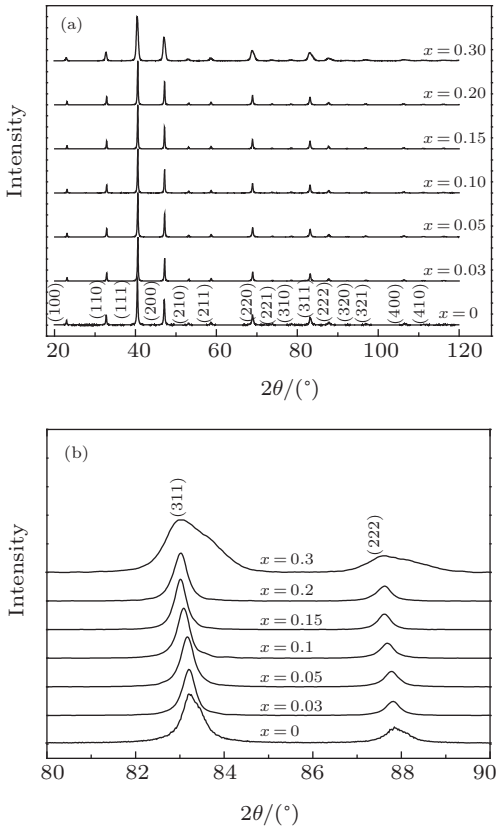


Fig. 1. (a) The PXRD patterns for the series of $Cd_{1-x}In_xNNi_3$ samples. (b) The enlarged portion of the reflections (311) and (222).

Figure 2 shows the PXRD patterns for the series of $Cd_{1-y}Cu_yNNi_3$ ($0 \leq y \leq 0.25$) samples. As shown in Fig. 2, the samples with $y \leq 0.2$ are single phase, while tiny impurity peaks (represented by the star and plus point) appear in the $Cd_{1-y}Cu_yNNi_3$ samples when $y > 0.2$. The impurity peaks are attributable to Cu_3N and metal nickel, so the limit of solid solubility of copper in the $CdNNi_3$ phase is slightly larger

than 0.2. From Fig. 3, it can be seen that the lattice parameter a of $Cd_{1-y}Cu_yNNi_3$ decreases and varies from 3.8483 Å to 3.8471 Å with the copper content increasing because of the smaller Cu atom generating a counteracting size effect. We tried to synthesize $CdNCu_3$ and $CuNNi_3$ compounds, but did not succeed under the present experimental condition.

The metal elemental content of the samples $Cd_{1-x}In_xNNi_3$ and $Cd_{1-y}Cu_yNNi_3$ were determined by EDX analysis. The analysis results are listed in Table 1. As shown in Table 1, the actual In:Cd, Cu:Cd, (Cd+In):Ni, and (Cd+Cu):Ni ratios are consistent with the stoichiometry within the experimental error, respectively. The elemental analysis shows that the nitrogen content of the prepared samples with x (or y) ≤ 0.2 is stoichiometric within the experimental errors.

Table 1. Elemental content determined by EDX analysis of the $Cd_{1-x}In_xNNi_3$ and $Cd_{1-y}Cu_yNNi_3$ samples.

Sample	M[a]/at%	Cd/at%	Ni/at%	N/at%	M:Cd	(Cd+M):Ni
$x = 0.05$	1.02	18.82	60.20	19.96	1:18.45	1.0:3.03
$x = 0.15$	3.01	17.07	59.89	20.03	1:5.67	1.0:2.98
$y = 0.05$	1.01	18.90	60.07	20.02	1:18.71	1.0:3.02
$y = 0.15$	3.02	17.03	60.04	19.91	1:5.64	1.0:3.00

[a] M represents In or Cu.

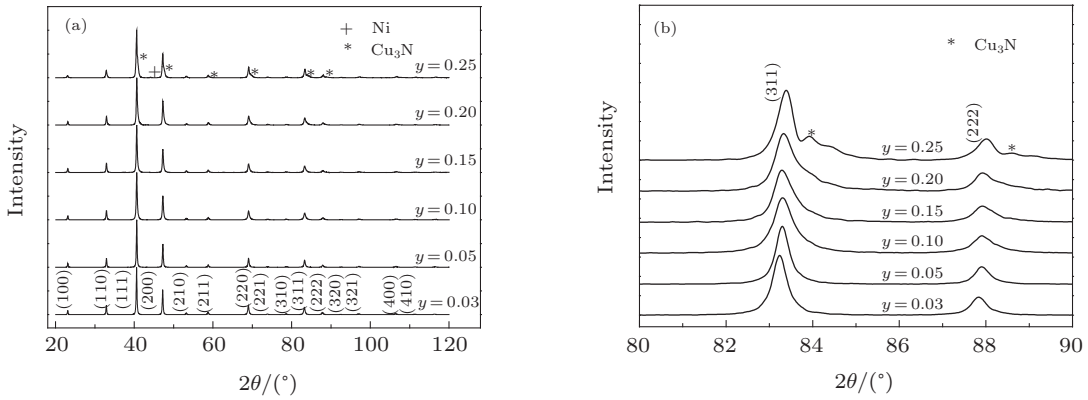


Fig. 2. (a) PXRD patterns for the series of $Cd_{1-y}Cu_yNNi_3$ samples. (b) The enlarged portion of the reflections (311) and (222).

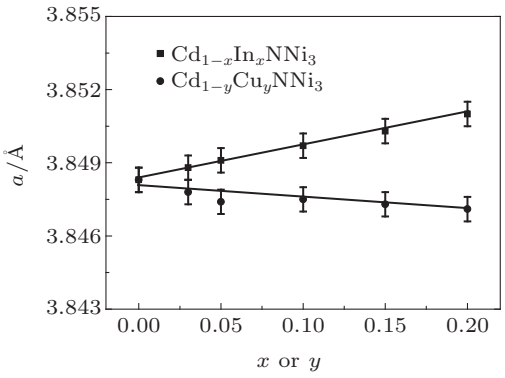


Fig. 3. Variation in lattice parameter a with the composition of the $Cd_{1-x}In_xNNi_3$ and $Cd_{1-y}Cu_yNNi_3$ samples. The solid lines represent linear fit.

The temperature dependence of the resistivity for the $Cd_{1-x}In_xNNi_3$ (x = 0, 0.1) and $Cd_{0.9}Cu_{0.1}NNi_3$ samples are shown in Fig. 4. Each sample exhibits metallic behaviors over the whole temperature range measured, and no superconductivity was found down to 5 K. At high temperatures ($T_F \sim 300$ K), the resistivity for the samples shows linear behavior, which is attributed to electron–phonon scattering. T_F is the onset temperature, where the sample deviates from linear behavior. Above T_F, the resistivity–temperature coefficient ($d\rho/dT$) of the three compounds has a relationship $d\rho/dT(Cd_{0.9}Cu_{0.1}NNi_3) < d\rho/dT(CdNNi_3) < d\rho/dT(Cd_{0.9}In_{0.1}NNi_3)$. The theoretical study has pointed out that the DOS of the $CdNNi_3$ has a large peak slightly below E_F.[21] According to the framework of rigid band approximation, Cu doping enhances $N(E_F)$, while In doping depresses $N(E_F)$, and as a consequence indirectly influences the conductivity. So the difference in conductivity for the $Cd_{1-x}In_xNNi_3$ (x = 0, 0.1) and $Cd_{0.9}Cu_{0.1}NNi_3$ samples could be explained by the changes in $N(E_F)$ caused by Cu or In doping. From the inset of Fig. 4, it can be seen that the resistivity of $Cd_{1-x}In_xNNi_3$ (x = 0, 0.1) and $Cd_{0.9}Cu_{0.1}NNi_3$ can be well fitted

with the equation:

$$\rho(T) - \rho_0 = AT^2 \tag{1}$$

in the range of 5 K $\leq T \leq T_{\rm F}$, which is suggestive of a Fermi liquid behavior. The fitting results are listed in Table 2. $Cd_{0.9}In_{0.1}NNi_3$ has a larger residual resistivity ρ_0 (103.1(3) μΩ·cm) than that of $Cd_{0.9}Cu_{0.1}NNi_3$ (83.7(2) μΩ·cm). This probably reflects the contributions from the extrinsic origins such as the grain boundaries[23] in $Cd_{0.9}In_{0.1}NNi_3$. Since our sample is polycrystalline, a quenched disorder of a certain amount cannot be ruled out, which comes from the extrinsic (such as grain boundaries and domain walls) and intrinsic (lattice defects and antisite disorders) disorders.

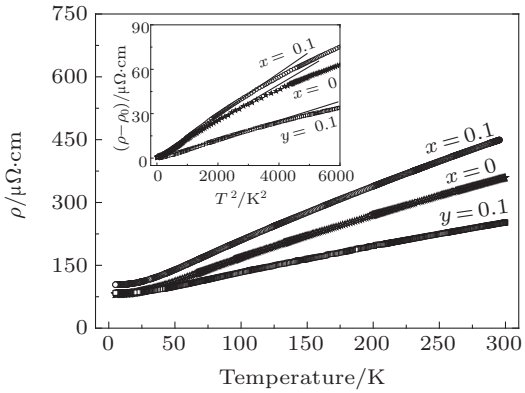


Fig. 4. The temperature-dependent resistivity of the $Cd_{1-x}In_xNNi_3$ and $Cd_{1-y}Cu_yNNi_3$ samples. Inset: the linear fitting of $\rho(T) - \rho_0$ versus T^2 below $T_{\rm F}$.

Table 2. The results of $Cd_{1-x}In_xNNi_3$ and $Cd_{1-y}Cu_yNNi_3$ fit to Eq. (1).

Sample	$T_{\rm F}$/K	ρ_0/μΩ·cm	A/(μΩ·cm/K^2)
$x = 0$	50(1)	80.7(2)	0.012(2)
$x = 0.1$	60(2)	103.1(3)	0.014(1)
$y = 0.1$	70(1)	83.7(1)	0.006(2)

Figure 5 depicts the temperature dependence of the magnetization of the $Cd_{1-x}In_xNNi_3$ and $Cd_{1-y}Cu_yNNi_3$ samples in zero-field cooled (ZFC) and field cooled (FC), respectively. There are two common features in their magnetization versus temperature curves. The first one is the divergence of the FC and ZFC curves, and the second one is that all ZFC curves exhibit a broad cusp. The irreversibility temperature ($T_{\rm irr}$), where the ZFC and FC curves diverge, shifts to the higher temperature with the increase in dopant content. As shown in Fig. 5(a), the ZFC curves of the $CdNNi_3$ sample show broad cusps at an applied field of 50 Oe (1 Oe=79.5775 A/m), and the cusps occur at temperature ($T_{\rm f}$) around 60 K. With the increase in applied field from 50 Oe to 1 kOe, the $T_{\rm f}$ of $CdNNi_3$ shifts toward lower temperature. The broad cusp ($T_{\rm f}$) in the ZFC curve can be attributed to the superparamagnetic blocking of spins.[24,25] The superparamagnetic blocking process is the competition between the thermal and anisotropy energies of the particles. It is clear that as the applied field increases, the anisotropy energy of the particles decreases. When this happens, the particles need less thermal energy to cross over the energy barrier and thus the $T_{\rm f}$ decreases. Simultaneously, the extent of irreversibility tends to vanish as the external field increases. From Figs. 5(b) and 5(c), it can be seen that $T_{\rm irr}$ increases as the dopant content increases for $Cd_{1-x}In_xNNi_3$ and $Cd_{1-y}Cu_yNNi_3$.

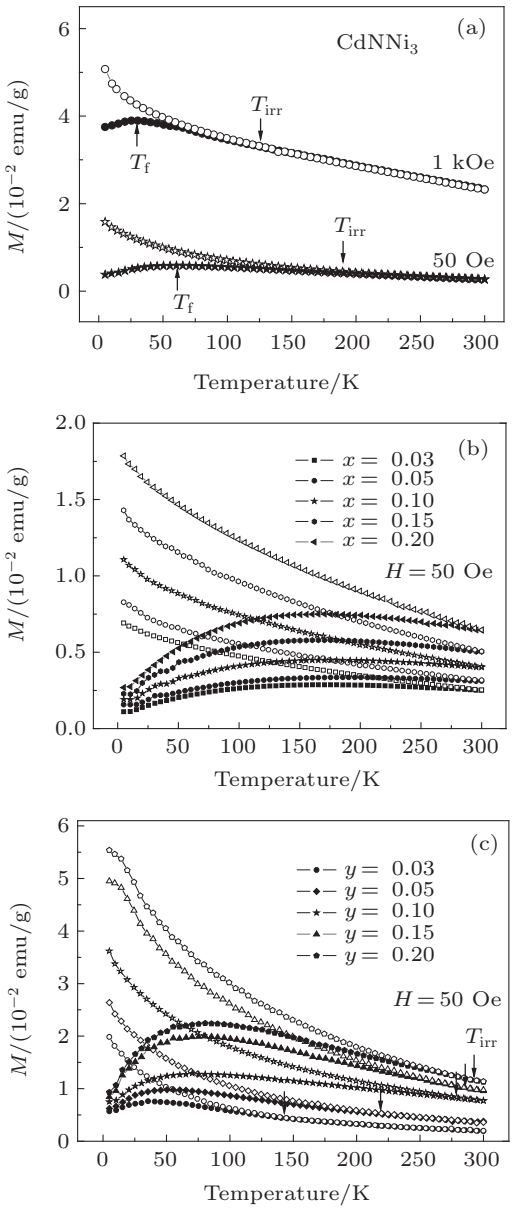


Fig. 5. Temperature dependence of the ZFC (filled symbols) and FC (open symbols) dc magnetization curves: (a) $CdNNi_3$, (b) $Cd_{1-x}In_xNNi_3$, and (c) $Cd_{1-y}Cu_yNNi_3$. The arrow symbols indicate $T_{\rm irr}$.

The $Cd_{1-x}In_xNNi_3$ ($x = 0.03$, 0.05, 0.10, 0.15, 0.20) samples show much higher irreversibility, as evidenced by significant splitting of the ZFC and FC curves at or near room temperature (Fig. 5(b)). Similar behavior is seen in frozen ferrofluids[26] and assemblies of nanoparticles.[27] The crystallite sizes of our samples are in the range of 50 nm–150 nm (Fig. 6), so the bifurcation in the ZFC and FC curves can be attributed to the presence of strong interactions between nanosized magnetic particles.[28] The T_{irr} shifts to the higher temperature with the increase in dopant content, which may be attributed to the increased anisotropy energies of the particles in the doped samples.

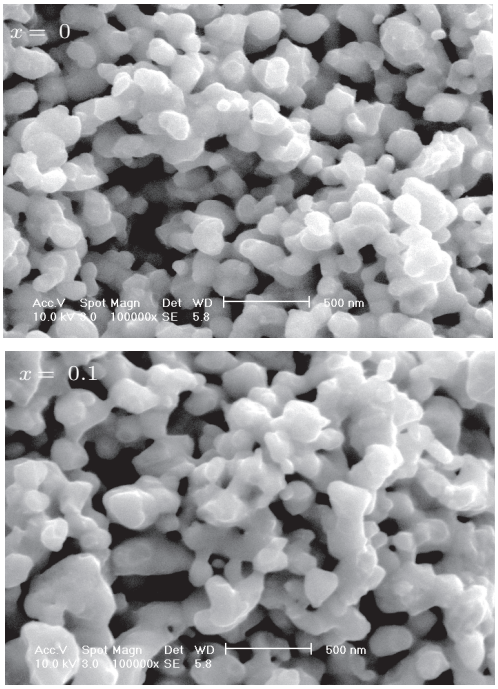


Fig. 6. SEM micrographs of the $Cd_{1-x}In_xNNi_3$ samples.

Figure 7 plots the hysteresis loops for the $CdNNi_3$, $Cd_{0.9}In_{0.1}NNi_3$, and $Cd_{0.9}Cu_{0.1}NNi_3$ samples at different temperatures (10 K, 150 K, and 300 K). The inset of Fig. 7 shows the isothermal $M(H)$ curves for the samples. From the hysteresis loops, we can see clearly that the coercivity and remanence of each sample decrease as the temperature increases. Above 150 K, each sample has very small coercivity and remanence, since its hysteresis loops are hardly visible. As shown in the inset of Fig. 7, the $M(H)$ curves of the $CdNNi_3$, $Cd_{0.9}In_{0.1}NNi_3$, and $Cd_{0.9}Cu_{0.1}NNi_3$ samples exhibit linear behavior at high magnetic field, indicating a PM response to the applied magnetic field, which may be due to spin pairing effects and the presence of superparamagnetic fractions (distribution of particle size).

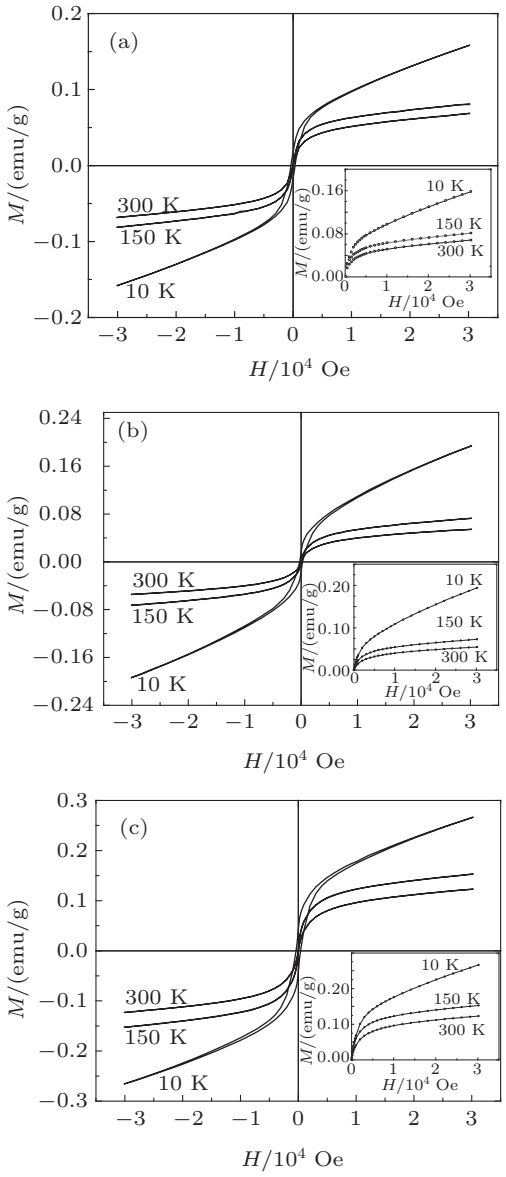


Fig. 7. Hysteresis loops at different temperatures: (a) $CdNNi_3$, (b) $Cd_{0.9}In_{0.1}NNi_3$, and (c) $Cd_{0.9}Cu_{0.1}NNi_3$. The inset shows the magnetization versus magnetic field isotherm (M–H) curves at different temperatures.

The Arrott plot technique was also used to determine the magnetic properties of the $CdNNi_3$, $Cd_{0.9}In_{0.1}NNi_3$, and $Cd_{0.9}Cu_{0.1}NNi_3$. Figure 8 shows the Arrott plot for the samples. The Arrott plot (M^2 against H/M) provides a useful criterion for the magnetic property, because a positive (negative) intercept on the ordinate of the extrapolated linear behavior in the high field portion corresponds to the ferromagnetic (paramagnetic) state. The intercepts for each sample are very close to the origin of the coordinate. Nonetheless, they are positive. So, each sample has very soft and weak ferromagnetism. For the $CdNNi_3$ sample, our result is different from the earlier report.[20] This difference indicates that the physical properties of the

$CdNNi_3$ sample are very sensitive to the synthesis routes and the variation in the compositions.

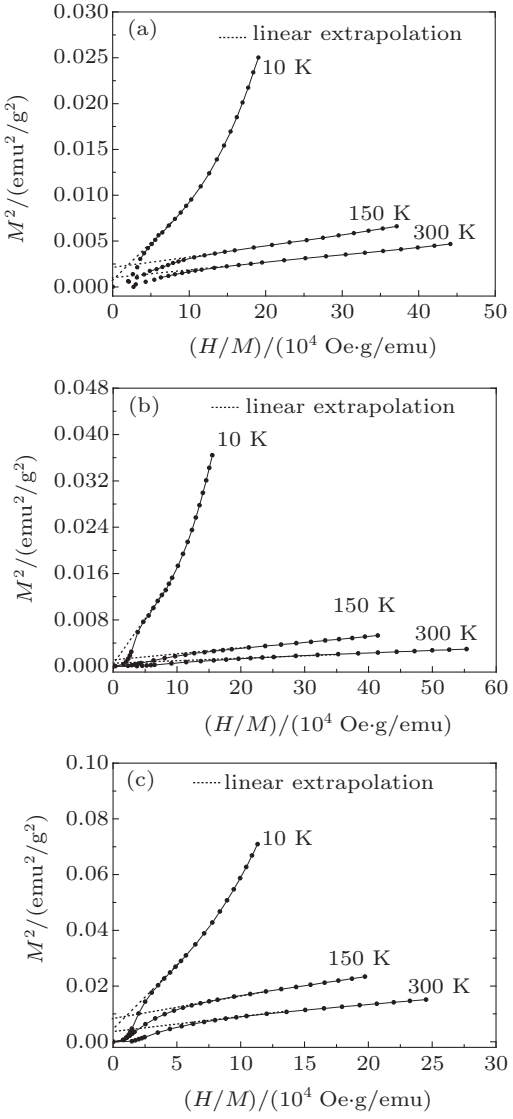


Fig. 8. Arrott plots [M^2–(H/M)] at different temperatures: (a) $CdNNi_3$, (b) $Cd_{0.9}In_{0.1}NNi_3$, and (c) $Cd_{0.9}Cu_{0.1}NNi_3$.

Figure 9 depicts the temperature dependence of the magnetization for $Cd_{1-x}In_xNNi_3$ and $Cd_{1-y}Cu_yNNi_3$ samples at a magnetic field of 50 Oe. The $M(T)$ curves of the $Cd_{1-x}In_xNNi_3$ and $Cd_{1-y}Cu_yNNi_3$ samples can be well fitted by using a combination of a Bloch law and a Curie–Weiss behavior.[29–31] The solid curves in Fig. 8 show the fitting results using the following equation:

$$M(T) = M_0[1 + B_0T^{3/2} + B_1T^{5/2}] + C/(T - \theta), \quad (2)$$

where B_0 and B_1 are spin wave parameters, because the spins are polarized to form spin–wave interactions in the ferromagnetic region. The Curie–Weiss behavior has been observed in interacting ferrofluids, where θ is a measure of the interaction strength.[32–34] The fitted parameters and the goodness of fit (R^2) are listed in Table 3. As can be seen in Table 3, the values of θ are negative and the values of M_0 increase with the increasing dopant concentration. The negative value for θ may be attributed to the antiferromagnetic ordering of the ferromagnetic particles when they aggregate. The changing trend of the M_0 values indicates that the effective magnetic moment per atom increases when the dopant content increases in these systems.

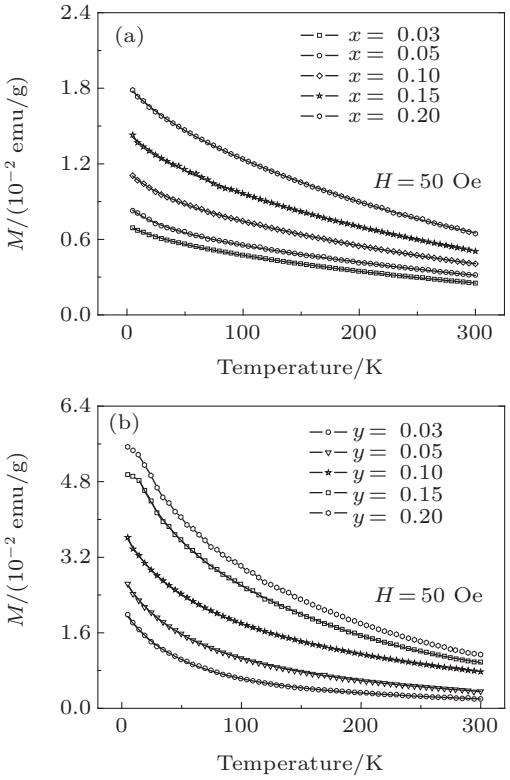


Fig. 9. Temperature dependence of magnetization at a magnetic field of 50 Oe: (a) $Cd_{1-x}In_xNNi_3$, and (b) $Cd_{1-y}Cu_yNNi_3$. The solid line represents the fit to Eq. (2).

From both resistivity and magnetic measurements, we find that the superconductivity is absent in the $Cd_{1-x}In_xNNi_3$ and $Cd_{1-y}Cu_yNNi_3$ samples down to 2 K. The main reason for the absence of superconductivity is attributed to the small $N(E_F)$ in these compounds. According to the theoretical study,[21,35] Ni 3d and a partial hybridization between Ni 3d and N 2p dominate the total DOS at E_F in the $MNNi_3$ (M = Mg, Zn, Cd, In). The component of M in the compounds has very small contributions to the $N(E_F)$. So the shift in the bands near the Fermi level of the $Cd_{1-x}In_xNNi_3$ and $Cd_{1-y}Cu_yNNi_3$ samples is very small and therefore indirectly influences the values of $N(E_F)$, resulting in the small value $N(0)$ in the samples. Further investigation of the electron–phonon coupling properties of the $CdNNi_3$ should be performed in order to elucidate its nature of absence of superconductivity.

Table 3. The results of $Cd_{1-x}In_xNNi_3$ and $Cd_{1-y}Cu_yNNi_3$ fit to Eq. (2).

Sample	M_0/(emu/g)	$B_0/K^{-3/2}$	$B_1/K^{-5/2}$	C/(emu·K/g)	θ/K	R^2
$x = 0$	4.30×10^{-3}	-4.21×10^{-3}	4.65×10^{-6}	0.66	−52	0.99992
$x = 0.03$	5.70×10^{-3}	-1.40×10^{-3}	1.2×10^{-6}	0.053	−36.5	0.99994
$x = 0.05$	6.10×10^{-3}	-1.31×10^{-3}	7.75×10^{-7}	0.087	−33	0.9997
$x = 0.10$	8.70×10^{-3}	-2.1×10^{-3}	1.61×10^{-6}	0.095	−33	0.99993
$x = 0.15$	1.15×10^{-2}	-3.11×10^{-3}	2.5×10^{-6}	0.12	−38	0.9997
$x = 0.20$	1.51×10^{-2}	-4.1×10^{-3}	3.4×10^{-6}	0.13	−40	0.99992
$y = 0.03$	9.80×10^{-4}	-1.31×10^{-3}	2.7×10^{-6}	0.93	−44	0.9995
$y = 0.05$	1.85×10^{-3}	-1.43×10^{-3}	1.75×10^{-6}	1.61	−61	0.99989
$y = 0.10$	1.36×10^{-2}	-4.4×10^{-3}	4.5×10^{-6}	1.35	−54	0.99983
$y = 0.15$	2.68×10^{-2}	-1.11×10^{-2}	1.0×10^{-5}	1.21	−37	0.99984
$y = 0.20$	3.39×10^{-2}	-1.35×10^{-2}	2.0×10^{-5}	1.03	−32	0.99983

4. Conclusion

In summary, the structure, magnetic and electronic transport properties of $Cd_{1-x}In_xNNi_3$ and $Cd_{1-y}Cu_yNNi_3$ have been investigated. The compounds with x (or y) ≤ 0.2 have the typical antiperovskite structure (space group $Pm3m$). $CdNNi_3$, $Cd_{0.9}In_{0.1}NNi_3$, and $Cd_{0.9}Cu_{0.1}NNi_3$ show metallic behavior in the temperature dependence of the resistivity from 5 K to 300 K. The temperature dependence of the magnetization and the hysteresis loops indicate that $CdNNi_3$, $Cd_{0.9}In_{0.1}NNi_3$, and $Cd_{0.9}Cu_{0.1}NNi_3$ have a soft and weak ferromagnetism below 300 K, respectively. The $CdNNi_3$ result is different from the report in the literature, which exhibits soft and weak ferromagnetic behavior. No superconductivity has been found in the $Cd_{1-x}In_xNNi_3$ and $Cd_{1-y}Cu_yNNi_3$ samples, which may be attributable to the small value $N(0)$. The physical properties of Ni-based antiperovskite nitrides are quite diversified and complicated, and further studies on their structure-property relations are needed.

References

[1] He T, Huang Q, Ramirez A P, Wang Y, Regan K A, Rogado N, Hayward M A, Haas M K, Slusky J S and Inumara K 2001 *Nature* **411** 54

[2] Uehara M, Amano T, Takano S, Kori T, Yamazaki T and Kimishima Y 2006 *Physica* C **440** 6

[3] Park M S, Giim J, Park S H, Lee Y W, Lee S I and Choi E J 2004 *Supercond. Sci. Technol.* **17** 274

[4] Tong P, Sun Y P, Zhu X B and Song W H 2006 *Phys. Rev.* B **74** 224416

[5] Tong P, Sun Y P, Zhu X B and Song W H 2006 *Phys. Rev.* B **73** 245106

[6] Tong P, Sun Y P, Zhu X B and Song W H 2007 *Solid State Commun.* **141** 33

[7] Matar S F, Mohn P, Demazeau G and Siberchicot B 1988 *J. Phys.* **49** 1761 (Paris)

[8] Matar S F, Demazeau G and Siberchicot B 1990 *IEEE Trans. Magn.* **26** 60

[9] Cordier–Robert C and Foct J 1992 *Eur. J. Solid State Inorg. Chem.* **29** 39

[10] Mohn P, Schwarz K, Matar S F and Demazeau G 1992 *Phys. Rev.* B **45** 4000

[11] Kuhnen C A, de Figueiredo R S, Drago V and da Silva E Z 1992 *J. Magn. Magn. Mater.* **111** 95

[12] Kuhnen C A and dos Santos A V 1993 *Solid State Commun.* **85** 273

[13] Kuhnen C A and dos Santos A V 1994 *J. Magn. Magn. Mater.* **130** 353

[14] Suzuki S, Sakamoto H, Minegismi J and Omote V 1981 *IEEE Trans. Magn.* **17** 3017

[15] Matar S F, Demazeau G, Hagenmuller P, Armitage J G M and Riedi P C 1989 *Eur. J. Solid State Inorg. Chem.* **26** 517

[16] Fruchart D and Bertaut E F 1978 *J. Phys. Soc. Jpn.* **44** 781

[17] Takenaka K and Takagi H 2005 *Appl. Phys. Lett.* **87** 261902

[18] Uehara M, Uehara A, Kozawa K and Kimishima Y 2009 *J. Phys. Soc. Jpn.* **78** 033702

[19] Cao W H, He B, Liao C Z, Yang L H, Zeng L M and Dong C 2009 *J. Solid State Chem.* **182** 3353

[20] Uehara M, Uehara A, Kozawa K and Kimishima Y 2010 *Physica* C **470** S688

[21] Li C, Chen W G, Wang F, Li S F, Sun Q, Wang S Y and Jia Y 2009 *J. Appl. Phys.* **105** 123921

[22] Dong C 1999 *J. Appl. Crystallogr.* **32** 838

[23] Yamaura K and Takayama-Muromachi E 2001 *Phys. Rev. Lett.* **64** 224424

[24] Sohn B H, Cohen R E and Papaefthyrniou G C 1998 *J. Magn. Magn. Mater.* **182** 216

[25] Zhang L, Papaefthymiou G C and Ying J Y 2001 *J. Phys. Chem.* B **105** 7414

[26] Luo W L, Nagel S R, Rosenbaum T F and Rosensweig R E 1991 *Phys. Rev. Lett.* **67** 2721

[27] O'Grady K, El–Hilo M and Chantrell R W 1993 *IEEE Trans. Magn.* **29** 2608

[28] Cieśak J, Costa B F O, Dubiel S M, Reissner M and Steiner W 2005 *J. Phys.: Condens. Matter* **17** 2985

[29] Yue L, Sabiryanov R, Kirkpatrick E M and Pelecky D L L 2000 *Phys. Rev.* B **62** 8969
[30] Dyson F J 1956 *Phys. Rev.* **102** 1217
[31] Pauthenet R 1982 *J. Appl. Phys.* **53** 2029
[32] Holmes M, O'Grady K and Popplewell J 1990 *J. Magn. Magn. Mater.* **85** 47
[33] Söffge F and Schmidbauer E 1981 *J. Magn. Magn. Mater.* **24** 54
[34] Dubovik V M, Martsenyuk M A and Martsenyuk N M 1995 *J. Magn. Magn. Mater.* **150** 105
[35] Hou Z F 2010 *Solid State Commun.* **150** 1874